Journal of Applied Polymer Science

Frontal Polymerization of Superabsorbent Nanocomposites Based on Montmorillonite and Polyacrylic Acid with Enhanced Soil Properties

Ruobing Zhang,[1] Zhaoxia Qiu,[2] Haixia Qiu,[1] Xionghui Zhang[1]

[1]Chemistry Department, School of Science, Tianjin University, Tianjin 300072, People's Republic of China

[2]Jincheng Landscape Research Institute, Jincheng, Shanxi 048000, People's Republic of China

Correspondence to: H. Qiu (E-mail: qhx@tju.edu.cn)

ABSTRACT: Polyacrylic acid/montmorillonite(MMT)/carboxymethylcellulose (CMC) superabsorbent nanocomposites were prepared by frontal polymerization (FP), an economic method characterized by low-energy consumption and short-reaction time. They were characterized by Fourier transform infrared spectroscopy, X-ray diffraction, transmission electron microscopy, and scanning electron microscopy. The effects of reaction parameters on the front propagation and the water absorbency of the nanocomposites were investigated. Furthermore, the effects of the obtained products on soil water holding capacity and soil water stable macro-aggregates were studied. Compared with the control soil, soil mixed with the nanocomposites showed a significant increase (by 52.4%) in field water holding capacity. The incorporation small amounts of MMT effectively promoted the formation of soil water stable macro-aggregates, which increased by 76% as the addition of the MMT increased to 4 wt %. The samples obtained by FP showed much better performance in the formation of soil water stable macro-aggregates, salt resistance, and thermal stability than those obtained by conventional batch polymerization. © 2013 Wiley Periodicals, Inc. J. Appl. Polym. Sci. **2014**, *131*, 39825.

KEYWORDS: gels; clay; composites; swelling; polysaccharides

Received 22 April 2013; accepted 7 August 2013

DOI: 10.1002/app.39825

INTRODUCTION

Frontal polymerization (FP) is a process of converting the monomer into polymer by means of a spatially localized reaction zone which propagates through the heat release by the reaction itself.[1] If the heat release is sufficiently higher than heat loss, the result is a self-sustaining hot front which propagates step by step through the reaction vessel.

In 1972, FP was first discovered by Chechilo and Enikolopyan. They studied methyl methacrylate polymerization in adiabatic conditions under high pressure.[2,3] Pojman et al. later demonstrated the feasibility of FP for a variety of monomers at ambient pressure.[4,5] The research of FP was widely reported in the last two decades. Free-radical polymerization is the most commonly used chemistry. The researchers found the possibility of achieving high monomer conversion in a short time which represented desirable features.[6–8] In order to avoid the formation of bubbles inside the polymer prepared via FP, Mariani et al. reported a new class of initiators based on ionic liquid compounds that resulted in lower temperature polymerization fronts.[9]

Several potential advantages of FP were found in some laboratories recently. Thermoresponsive poly(*N*-vinylcaprolactam) nanocomposite hydrogels containing high concentration of graphene were successfully prepared via FP by Sannal et al.[10] Zhou et al. described a facile fabrication of white light-emitting CdS/polymer nanocomposites via plasma-ignited FP.[11] Singh et al. achieved the synthesis of CdS nanoparticles in polymer matrix via FP.[12]

Superabsorbent polymers (SAPs) are lightly crosslinked three dimensional networks, which have the ability to absorb considerable amount of water (tens to thousands of times their own weight) in a relatively short time and have good water-retention capacity. They have been widely applied in personal hygiene products such as disposable pads and towels used in surgery. Moreover, SAPs have many practical applications in agriculture and horticulture. They are used as soil additives to increase the soil water holding capacity, improve the soil structure, and promote the formation of soil aggregates.[13,14] In particular, the addition of SAPs to soils greatly reduces the irrigation frequency, which could be best utilized for water conservation in arid and semi-arid regions.[15]

FP has been used to prepare SAPs in recent years. A starch-graft-sodium acrylate-*co*-acrylamide superabsorbent prepared using FP was described by Yan's group.[16] Later the group

produced other superabsorbent hydrogels based on acrylic acid (AA) monomers grafted onto starch via FP. They studied the effects of temperature and tube size on propagating front and properties of hydrogels.[17] Li et al. used FP to prepare two kinds of SAPs based on konjac glucomannan and polyacrylic acid (PAA), which had high absorbing capacity in distilled water and physiological saline.[18]

Carboxymethyl cellulose (CMC) is a representative cellulose derivative with carboxymethyl groups bound to some of the hydroxyl groups on the cellulose backbone. The polar carboxyl groups render the cellulose soluble, chemically reactive, and strongly hydrophilic. It is a natural organic polymer that is non-toxic and biodegradable. It is also cheap and readily available. The above properties make it ideal for industrial applications especially the superabsorbent fields.[19]

Montmorillonite (MMT) is a kind of loose-layer silicate made up of two tetrahedral sheets fused to an edge-shared octahedral sheet of aluminum hydroxide, with a thickness of ~1 nm and a length of ~100 to several 100 nm. It has high cation-exchange capacities. MMT is widely used in the field of nanometer polymeric materials because of its good dispersibility. Polymer/MMT nanocomposites are materials based on the intercalation of polymer chains into MMT layers; they often exhibit remarkable improvement in materials properties when compared with conventional composites. Because of its hydrophilic nature, MMT is suitable for use in SAPs as additives. The addition of MMT can improve the gel strength and water absorption rate of the SAPs.[20,21] However, SAPs/MMT nanocomposites prepared by FP have not yet been reported.

In our previous work, PAA/MMT/CMC superabsorbent nanocomposites with good water retention ability were prepared using conventional batch polymerization.[22] However, the preparation process is time-consuming: (i) The inhibitor from AA monomer should be removed by distillation under reduced pressure before use, otherwise the polymerization process would be delayed; (ii) The reaction time is too long (>4 h) to achieve high monomer conversion.

The significant advantages of FP are low energy consumption (it does not need external energy supplying but an initial input of heat, whereas in conventional polymerization techniques, external energy supplying is necessary for complete experiment duration) and shorter reaction time (a few minutes instead of hours in conventional polymerization). In addition, FP has several other potential advantages over conventional polymerization: (i) Because of the high temperature reached by the propagating fronts, polymerization runs can be performed without removing the inhibitor from the monomers; (ii) Waste production can be reduced by eliminating post polymerization solvent removal; (iii) FP can avoid thermal runaway polymerization. Moreover, some properties of FP products are better than those materials traditionally obtained due to the high temperatures reached by the propagating fronts.

Taking into account all previous considerations, in this study, we attempted to prepare PAA/MMT/CMC superabsorbent nanocomposites by FP. Though there have been a few reports of SAPs prepared by FP recently,[16–18] no study involving the investigation of FP products on soil physical properties has been reported so far. Effects of the obtained products on soil physical properties including water holding capacity, total porosity, and soil water stable macro-aggregates were also investigated and compared with analogous materials prepared by the conventional method. The investigation of SAPs on soil physical properties is essential for their potential application in agriculture.

EXPERIMENTAL

Materials

MMT, CMC, sodium hydroxide (NaOH), sodium chloride (NaCl), calcium chloride ($CaCl_2$), and aluminum chloride ($AlCl_3$) were purchased from Tianjin Windship Chemistry Technological Co., Ltd. Potassium persulfate (KPS), *N*,*N*-methylene bisacrylamide (NMBA), and AA were purchased from Tianjin Damao Chemical Reagent Factory. They were all of A.R. grade and used without further purification.

Preparation of PAA/MMT/CMC Superabsorbent Nanocomposites

AA (10 g) was neutralized in an ice bath with 40 wt % NaOH until the neutralization was 60% complete on a molar basis. MMT (>200 mesh) and distilled water were mixed and ultrasonic dispersed for 10 min. A solution of CMC was added to the MMT suspension and the mixture was stirred vigorously for 20 min. Then, solutions of the partially neutralized AA, the initiator (KPS), and the crosslinker (NMBA) were added to the MMT–CMC mixture and stirred magnetically at room temperature for 20 min.

The prepared reactant mixture was poured into a 180 mm (*D* 18 mm) long test tube, which was clamped to an iron support in a drying oven at reaction temperature (30°C) for 30 min. FP was initiated by putting a hot soldering iron on the top of the tube until the formation of the traveling front became evident. After the reaction was complete, the tube was removed from iron support and cooled to room temperature. The reaction product was cut into small pieces and immersed in ethanol for 24 h to remove the unreacted monomer. The pieces were dehydrated under the infrared lamp, crushed into powder and finally dried to a constant weight at 70°C in a vacuum oven.

Frontal Velocity and Temperature Measurements

The frontal velocities were determined by measuring the distance that the front traveled as a function of time, which was in terms of centimeters per minute (cm/min). The temperature change was recorded by a K-type thermocouple (TES1310-TYPE), which was immersed at a 4.0 cm distance from the free surface.

Water Absorbency Measurements

Water absorbency measurements were performed at room temperature by a filtration method. A fixed amount (0.10 g) of fractionated (60–80 mesh) products were put in nylon bags and immersed in 200 mL of distilled water or salt (NaCl, $CaCl_2$, and $AlCl_3$) aqueous solutions until equilibrium had reached, then

the swollen samples were filtered for 10 min. The absorption extent of SAPs was calculated as:

$$Q_i = (m_t - m_0)/m_0 \quad (1)$$

where m_0 is the weight of dried absorbent and m_t is the weight of swollen absorbent after absorption.

Measurements of the Water Holding Capacity and Total Porosity of the Soil

The soil used was collected from Tianjin, China. It was air-dried and sieved through a 2-mm screen. Maximum/capillary/field water holding capacity was determined in the laboratory using the Cutting Ring method (Wilcox method).[23,24] The sieved soil samples were mixed with PAA/CMC/MMT nanocomposites (0.3 wt % based on soils) and put into different plastic basins. Then an equal amount of tap water (1200 mL) was added according to the water content in the field. Soil samples were taken out from plastic basins using a metallic cutting ring of known internal volume (100 cm^3). The soil cutting rings were saturated with tap water for 12 h, water in the soil represented the maximum water-holding capacity; then the surplus water was sucked off for 2 h using a dried sand-bed, and the remaining water in the soil was the capillary water holding capacity; after the surplus water was further sucked off for 72 h using a sand-bed, the remaining water in the soil was the field water holding capacity. The Cutting Ring method was also used to measure the total porosity of the soil.[24] The soil without SAPs was used as the control.

Water Absorbency Under Load

About 0.20 g sample was spread uniformly in a weighted glass tube (D 10 mm) with one end sealed with a 280 mesh fabric, and then a 9.00 g glass cylinder was placed on the sample ($P \approx 1.1 \times 10^3$ Pa). Then put it into a beaker containing distilled water for 24 h at room temperature. The water absorption extent under load was calculated according to the following equation:

$$Q_p = (m_2 - m_1 - m_0)/m_0 \quad (2)$$

where m_0 donates the weight of dry sample, m_1 is the weight of glass tube and load. m_2 donates the weight of glass tube with the swollen hydrogel and load.

Determination of Soil Water Stable Macro-Aggregates Distribution

Wet-sieving method was used to determine the content of soil water stable macro-aggregates.[25] After 0.3 wt % SAPs were added to the air-dried soil (one control sample without SAPs), it was shaken in a set of sieves with apertures of 10, 7, 5, 3, 2, 1, 0.5, and 0.25mm from top to bottom to separate the soil to different sizes. About 50.00 g soil samples composed of the same weight percentage of the dry-sieving samples were obtained. The samples as well as appropriate amount of water were put in a settling vat and thoroughly mixed. And then samples were poured onto a set of sieves with apertures of 5, 3, 2, 1, 0.5, and 0.25 mm and thoroughly mixed. The soil sample from each sieve was transferred to an aluminum can, dried, and weighed. The content of soil aggregate was calculated according to eq. (3):

$$\%\text{Soil aggregate} = m_i/m_0 \times 100 \quad (3)$$

where m_i and m_0 were the weight of soil aggregates with different levels and that of dried soil samples, respectively.

The mean grain size was defined by eq. (4):

$$\text{Mean grain size} = \sum N_i \cdot X_i \quad (4)$$

where N_i and X_i were the grain size and mass fraction of each level, respectively.

Characterization

Fourier transform infrared spectroscopy (FTIR) of the samples were recorded on a BIO-RAD 3000 FTIR spectrometer using KBr pellets at a resolution of 4 cm^{-1} in the range of 400–4000 cm^{-1}. X-ray powder diffraction (XRD) measurement was carried out on a Rigaku (Japan) DMAX-RC diffractometer operating at 100 mA and 40 kV using a Co K_α as radiation source (λ = 0.1790 nm). Transmission electron microscope (TEM) experiments were carried out on a Philips-EM400SP TEM. Samples were cut using LKB5 microtome with an average thickness of 80–100 nm. The microstructure of a dry SAP sample was also investigated by means of a scanning electron microscope (SEM, Philips XL-30M). The samples used for the SEM measurements were coated with gold. The differential scanning calorimetry (DSC) of the samples were performed in dynamic nitrogen atmosphere on a TG-DSC STA 409 PC (NETZSCH, Germany) in the temperature range 30–700°C at a heating rate of 10 K/min.

RESULTS AND DISCUSSION

Effects of MMT and CMC Content on FP

Table I shows the effect of different condition on front propagation. As shown in Table I, the front velocity decreased rapidly from 1.26 to 0.63 cm/min and maximum temperature (T_{max}) decreased from 113 to 104°C as the MMT/AA ratio increased from 0 to 3 wt %. MMT may be considered as an inert component in this system, so the presence of MMT can significantly affect the heat transfer performance of the mixture. With a higher MMT loading, more filler is available to absorb heat from the propagating front and, consequently, a decrease in front velocity and T_{max} will occur.

T_{max} was almost the same when MMT/AA ratio increased from 2% to 4%. The value of T_{max} relates to the heat release and heat loss during the polymerization process. Because of the relatively low reactivity of MMT, the heat release from polymerization decreased with the increase of MMT. The heat loss includes heat loss from heat transfer and heat loss from convection. With the increase of MMT, the former increased as MMT was unfavorable to heat transfer, while the later decreased because of the increase in viscosity of polymerization system. The significant viscosity increase of polymerization system decreased the heat loss from convection effectively when MMT/AA ratio increased from 2 to 4%, which counteracted the decrease of polymerization heat and the increase of heat loss from heat

Table I. Effect of Different Condition on Front Propagation and Water Absorbency

No.	MMT/AA (wt/wt)	CMC/AA (wt/wt)	KPS/AA (wt/wt)	MBA/AA (wt/wt)	Velocity (cm/min)	T_{max} (°C)	Water absorbency (g/g)
FP1	0	0.01	0.015	0.001	1.26	113	304
FP2	0.01	0.01	0.015	0.001	1.05	111	393
FP3	0.02	0.01	0.015	0.001	0.83	103	435
FP4	0.03	0.01	0.015	0.001	0.63	104	643
FP5	0.04	0.01	0.015	0.001	0.67	105	476
FP6	0.05	0.01	0.015	0.001	-	-	-
FP7	0.03	0	0.015	0.001	-	-	-
FP8	0.03	0.005	0.015	0.001	0.78	109	413
FP9	0.03	0.015	0.015	0.001	0.89	105	454
FP10	0.03	0.02	0.015	0.001	-	-	-
FP11	0.03	0.01	0.01	0.001	-	-	-
FP12	0.03	0.01	0.02	0.001	1.07	114	384
FP13	0.03	0.01	0.025	0.001	1.23	116	261
FP14	0.03	0.01	0.015	0.0015	0.85	107	446
FP15	0.03	0.01	0.015	0.002	0.86	125	438

transfer originated from the increase of MMT content, as a result, T_{max} didn't change significantly.

When MMT content reached 5 wt %, the polymerization mixture viscosity was increased, this decreased the probability of collision of monomers and crosslinker to the reactive growing polymer chain,[26] the heat of polymerization released from per unit volume decreased. In addition, high MMT content is unfavorable to the heat transfer of the propagating front. As a result, the heat loss is higher than heat release and the propagating front couldn't be sustained.

No propagation front was observed in the absence of CMC (Table I, FP7).The viscosity of the polymeric solution without CMC was low, so heat loss from convection eventually quenched the propagation front. Addition of CMC increased the viscosity of the system so that convection was minimized. In addition, proper amount of CMC increased the dispersion degree of MMT by intercalating into the layers of MMT,[22] which was also beneficial to obtain a stable front. However, too much CMC could quench a propagating front due to the high viscosity at higher CMC content (FP10), since high viscosity is unfavorable to heat transfer, which made energy from the exothermic polymerization difficult to diffuse into the adjacent region. The front velocity and T_{max} exhibited a minimum at the 1 wt % of CMC based on the weight of AA (FP4).

Effects of Initiator and Crosslinker Concentration on FP

Reaction could not be triggered when ratio of initiator/AA was below 1 wt % (FP11), which indicated that the low initiator concentration could not sustain the propagation of front. Front velocity increased with increasing the amount of initiator, from 0.63 to 1.23 cm/min, as a result of enhanced radical concentration (Table I). The increase of initiator concentration caused an increase of T_{max} from 104 to 116°C. The experiments were all performed under nonadiabatic conditions and the higher velocity would reduce heat loss, so that the dependence of T_{max} on initiator was similar as front velocity. Besides, in comparison to conventional polymerization, FP could overcome the polymerization inhibition of monomer so as to allow polymerization at lower initiator concentration.

As shown in Table I, the T_{max} and front velocity both increased with increase in crossslinker which would have affected the heat transmission from the system.

Effect of MMT Content on the Water Absorbency of SAPs

The water absorption of SAPs kept increasing from 304 to 643 g/g with the increasing ratios of MMT/AA from 0 to 3 wt % (Table I). The increase in water absorption could arise from the strong chemical interaction among MMT, CMC, and PAA, which could be confirmed by FTIR spectra.

Figure 1 shows comparative analysis of the FTIR spectra from CMC, MMT, PAA, and PAA/CMC/MMT nanocomposite FP4. The characteristic vibration bands of CMC were shown at 3240 cm^{-1} (stretching vibration of —OH), 1589 cm^{-1} (asymmetric vibration absorption of —COO^-), 1323 cm^{-1} (—OH bending vibration), 1020 cm^{-1} (cellulose ether linkage stretching vibrations).[27] AA was partially neutralized to acrylate, absorption of C═O stretching of COOH and COO^- were both observed in the spectrum of PAA. The weak band at 1678 cm^{-1} was the C═O stretching of —COOH, asymmetric vibration absorption of —COO^- occurred at 1562 cm^{-1}, the bands around 1321 and 1068 cm^{-1} were assigned to —OH bending vibration and C—O asymmetric stretching, respectively.

In the spectrum of PAA/CMC/MMT nanocomposite FP4 [Figure 1(d)], the absorption band at 1068 cm^{-1} of PAA disappeared, the weak band at 1678 cm^{-1} of PAA shifted to higher wavenumber at 1709 cm^{-1} as well as an increase in intensity, the band at 1562 cm^{-1} of PAA shifted to 1568 cm^{-1}, suggesting that —COOH, —COO^- groups of PAA participated in chemical

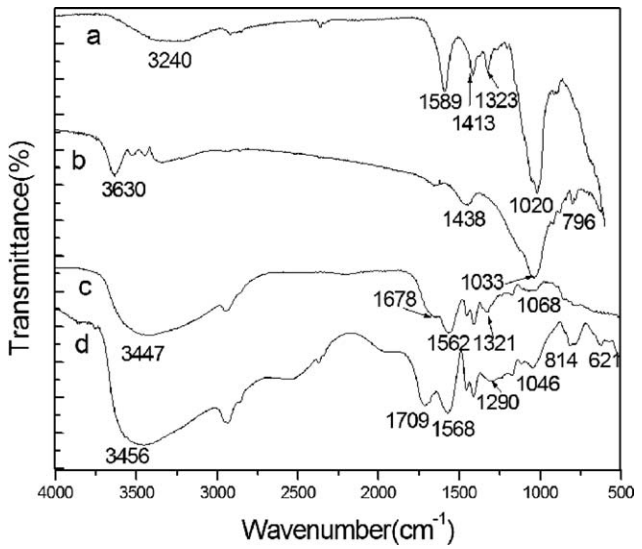

Figure 1. FTIR spectra of CMC (a), MMT (b), PAA (c), and PAA/CMC/MMT nanocomposite FP4 (d).

reaction; the characteristic absorption bands of CMC at 1020 cm^{-1} disappeared, the bands at 1323 cm^{-1} of CMC and 1321 cm^{-1} of PAA overlapped with each other and moved to 1290 cm^{-1}, indicating that ether bonds and —OH groups of CMC participated in chemical reaction; the band at 3630 cm^{-1} which was assigned to —OH stretch of MMT disappeared, the absorption band at 1033 cm^{-1} (stretching vibrations of Si—O of MMT) moved to 1046 cm^{-1} and it turned to be much weaker, the peak at 796 cm^{-1} due to Al—O stretch of MMT was split apart into two peaks at 814 and 621 cm^{-1}. FTIR spectra indicated the strong chemical bonding among Si—O, Al—O, and —OH groups of MMT sheets and functional groups of PAA (—COOH, $—COO^-$ groups) and CMC (ether bonds and —OH groups), which was one of the causes leading to high water absorption rate. Figure 2 shows the proposed mechanistic pathway for synthesis of superabsorbent nanocomposites.

In addition, as discussed above, MMT reduced T_{max} and front velocity effectively, which made the molecular weight of the SAPs increase and consequently improved their water absorption performance. Meanwhile, MMT also became the crosslink points of the water absorbency network at low content, thus leading to the expanding of the water absorbency network.[28] However, water absorbing capacity decreased rapidly with the increasing ratio of MMT/AA from 3 to 4 wt %. This was probably owing to the crosslinking property of MMT it owns, which might lead to the over-crosslinking of the SAPs.

Effect of the Amount of CMC on the Water Absorbency of SAPs

Water absorption extent increased from 413 to 613 g/g as the CMC/AA ratio increased from 0.5 to 1.0 wt % (Table I). CMC has hydrophilic groups such as hydroxyl and carboxylate groups, which are beneficial in improving water absorption capacity of SAPs. The dispersion degree of MMT in the polymer matrix greatly influences the water absorbency of superabsorbent

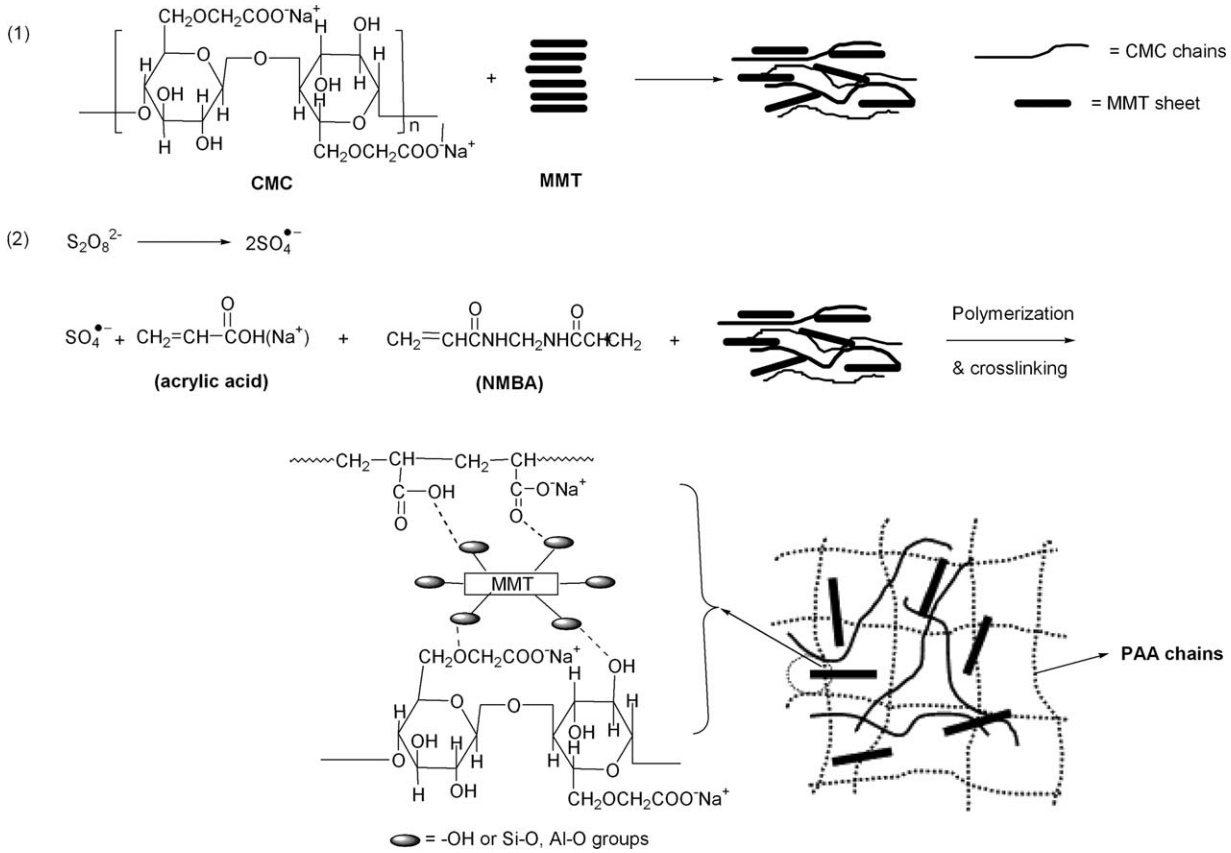

Figure 2. Proposed mechanistic pathway for synthesis of superabsorbent nanocomposites.

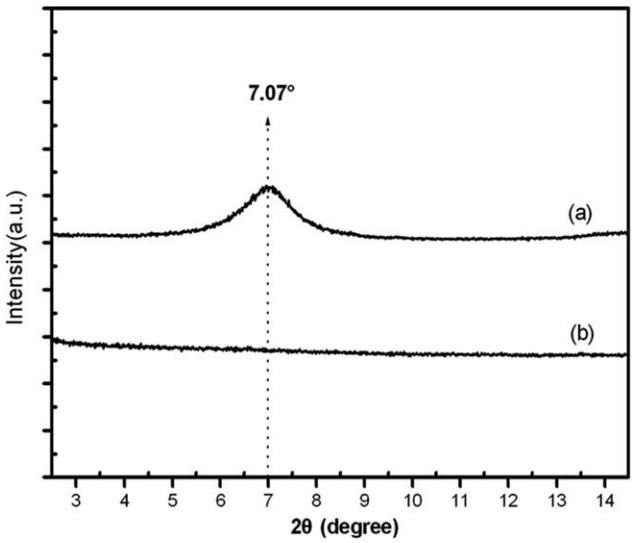

Figure 3. XRD patterns of pure MMT (a) and PAA/CMC/MMT nanocomposite FP4 (b).

composites.[29] The larger interactions between MMT and PAA lead to agglomeration of MMT which was seen as agglomerated mass at the bottom of the reaction tube. The presence of CMC could greatly improve the dispersion degree of MMT, which also contributed to the increase of water absorbency.

The good dispersion of MMT in PAA/CMC/MMT composites could also be evidenced from XRD and TEM analysis. The XRD patterns shown in Figure 3 are the pure MMT and PAA/CMC/MMT nanocomposite (FP4), respectively. For MMT, a prominent peak corresponding to the basal spacing of MMT occurred at a *d*-spacing 1.25 nm ($2\theta = 7.07°$).[30] This peak disappeared in the PAA/CMC/MMT composite, indicating that the MMT layers were exfoliated and dispersed in nanoscale in PAA matrix.

TEM observations were used to further in augment XRD analysis of the nanostructures. As shown in Figure 4, the brighter region represents the polymer matrix while the dark narrow stripes represent the MMT nanosheets. It shows that some individual layers of MMT are dispersed in the PAA matrix and separated one from another. This means that MMT is exfoliated on nanoscale and exists in the form of an intercalated structure, which is in accordance with XRD analysis.

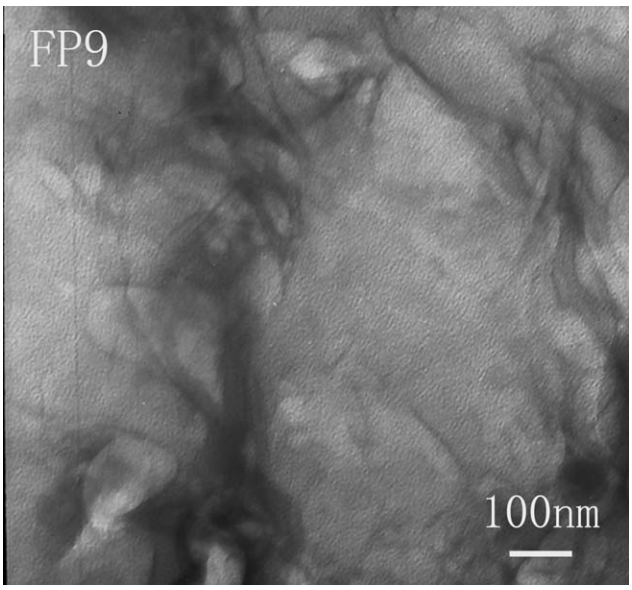

Figure 4. TEM image of PAA/CMC/MMT nanocomposite FP9.

With the increase of CMC/AA ratio from 1% to 1.5 wt %, the water absorption extent decreased. When excessive amount of CMC was added, the viscosity of the reaction system increased significantly, interaction of monomer with growing polymer PAA chain decreased and consequently the water absorption extent decreased. Excessive amount of CMC increased the number of physical crosslinks that result from the entanglement between CMC and PAA chains, which also resulted in the decrease of water absorption.

Effects of Initiator and Crosslinker Concentration on the Water Absorbency of SAPs

From Table I, it can be seen that the water absorption decreased rapidly from 643 to 261 g/g as the initiator/AA ratio was raised from 1.5 to 2.5 wt %. The polymerization rate increased with increasing initiator concentration, so heat from polymerization was not easy to dissipate, leading to excessive crosslinking and consequently decrease of water extent. In addition, the molecular weight of the polymer decreased with increasing initiator, which also led to decrease in swelling extent.

The amount of crosslinker could affect crosslinking degree of the final products[31] and subsequently affect the water absorbency and microstructure. As shown in Table I, greater absorbency (643 g/g) was obtained at the crosslinker/AA ratio was 0.1 wt %. High crosslinker concentration generated more crosslink points in the polymeric network and made the water absorbency decrease.[32]

Effect of SAPs on the Water Holding Capacity and Porosity of Soils

For agricultural purposes, evaluation of the efficacy of SAPs in absorbing water is of limited value when performed in the absence of soil material.[33] Table II shows the maximum/capillary/field water holding capacity of soils mixed with different PAA/CMC/MMT nanocomposites. BP4 is a reference sample synthesized using batch polymerization (BP), which has the same composition as that of FP4. Comparisons among the different samples reveal that soil mixed with FP9 exhibited the highest maximum/capillary/field water holding capacity. Compared with the control soil, FP9 modified soil showed a significant increase (by 52.4%) in field water holding capacity, which is very important for plant growth because improvement in field water capacity increases the available water to plants. Although FP4 sample emerged as the most effective SAPs in the distilled water system (Table I), FP4 soil showed lower maximum/capillary/field water holding capacity than that of FP9. We speculate that this may be due to the cations (Ca^{2+}, Mg^{2+}, Fe^{3+}, Al^{3+}) present in the soil and the pressure created by the soil particles surrounding the SAPs grains, which greatly influenced the water absorbency of SAPs.[34,35] In order to verify this, following tests were carried out.

The water absorption extent under load (Q_p) of FP4, FP9, and BP4 are shown in Figure 5. Q_p of FP9 was higher than FP4 because the long chains of CMC could physically entangle on

Table II. Soil Water Holding Capacity and Soil Total Porosity of FP, BP, and Control Samples

Sample	Maximum water holding capacity (g/kg)	Capillary water holding capacity (g/kg)	Field water holding capacity (g/kg)	Total porosity (vol%)
FP1	509.4	456.4	238.4	63.2
FP3	536.2	495.4	262.6	60.7
FP4	510.9	480.3	273.1	61.4
FP5	529.8	499.1	301.2	60.5
FP8	551.8	516.4	314.9	61.0
FP9	581.8	539.5	316.7	62.2
BP4	556.5	516.0	296.2	61.1
Control	473.7	437.5	207.7	56.8

SAP network, thus enhances the elasticity of network, which would retain the pore structure effectively.[36] The rigid network of BP4 made its Q_p higher than FP4. Thus, the soil water holding capacity of FP4 was not such outstanding comparing to its water absorbency extent.

The influence of cations on swelling capability of SAPs was studied by the addition of different saline solutions, including monovalent (NaCl), divalent ($CaCl_2$), and trivalent ($AlCl_3$) ions with different concentrations. As shown in Table III, the uptake for the nanocomposites in the studied salt solutions is in the order of monovalent > divalent > trivalent cations. The uptake capacity decreased significantly with the increase in concentration of salt solutions, which may be attributable to the reduction of the osmotic pressure (Na^+) and the increase of the crosslinking points (Ca^{2+}, Al^{3+}).[37] What should be pointed out is that the performance of FP9 is prominent, especially in NaCl and $CaCl_2$ solutions, which is in accordance with data of water holding capacity in Table II.

SAPs are usually used in saline atmosphere. Table III shows that the water absorbency of FP4 sample was higher than that of BP4 in NaCl and $CaCl_2$ solutions(especially in NaCl solutions), indicating that FP products possessed better salt resistance performance than BP samples, which provides a new way to improve the salt resistance of SAPs.

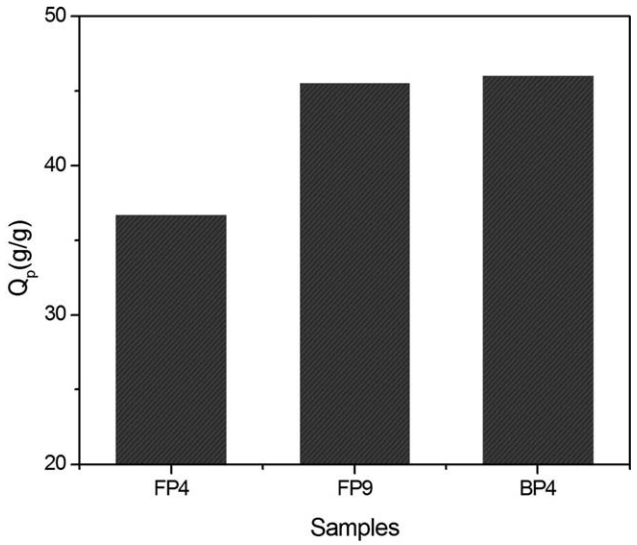

Figure 5. Water absorption extent under load (Q_p) of FP4, FP9, and BP4.

The soil porosity is another significant parameter as it is the transport channel of soil water and air. As shown in Table II, total porosity of the soils mixed with PAA/CMC/MMT nanocomposites was higher than that of the control soil, no significant difference was observed between FP4 and BP4.

Effect of SAPs on Soil Water Stable Macro-Aggregates Distribution

Soil aggregation is a crucial soil property affecting soil stability and crop production. The soil water stable macro-aggregates are aggregates whose diameters are between 2.5 mm and 10.0 mm in the soil. The presence and abundance of water stable macro-aggregates may reduce the soils structural degradation in the form of compaction, surface crusting, and sheet erosion.[38] As shown in Table IV, with increase in MMT content, the total amount and mean grain size of aggregates also increased. This result indicated that the incorporation of very small amounts of MMT to SAPs effectively promoted the formation of soil water stable macro-aggregates.

MMT is exfoliated into nanosheets in polymer matrix (Figure 4), the nano-dispersed MMT sheets exhibited large specific surface areas and strong surface energy, which enabled them to coalesce soil aggregates together by surface complexation. In addition,

Table III. Water Absorbency of FP, BP, and Control Samples at Different Salt Solutions

	Water absorbency (g/g) at salt aqueous solutions with different concerntrations								
	NaCl(mmol/L)			$CaCl_2$(mmol/L)			$AlCl_3$(mmol/L)		
Sample	1	5	10	1	5	10	1	5	10
FP1	270	170	156	203	63	18	181	26	25
FP3	329	221	168	220	67	23	219	31	25
FP4	323	215	190	228	72	33	221	30	32
FP5	326	225	177	215	76	40	200	30	33
FP8	321	227	202	253	76	49	235	29	32
FP9	340	234	210	275	82	50	229	30	33
BP4	180	165	113	225	64	23	227	31	31

Table IV. Aggregates Size Distribution of FP, BP, and Control Samples

No.	%Total soil macro-aggregates	% Soil water stable macro-aggregate distribution						Mean grain size (mm)
		0.25–0.5 (mm)	0.5–1.0 (mm)	1.0–2.0 (mm)	2.0–3.0 (mm)	3.0–5.0 (mm)	>5.0 (mm)	
FP1	19.2	52.4	42.9	1.9	1.1	1.8	0	0.65
FP3	26.3	48.5	40.6	7.0	1.2	2.6	0	0.73
FP4	30.1	41.4	41.9	12.0	2.1	2.2	0.3	0.81
FP5	33.8	34.1	45.0	13.4	2.5	4.3	0.7	0.94
FP8	37.9	33.0	44.3	16.8	2.3	3.5	0	0.91
FP9	35.3	34.3	45.5	14.5	2.5	3.3	0	0.88
BP4	18.3	42.1	46.6	8.2	1.8	1.4	0	0.73
Control	11.1	50.0	36.1	11.3	0.4	2.2	0	0.73

MMT sheets has cation adsorption capacity because their excess negative charges in both the octahedral and the tetrahedral sheets due to the exchange of structural Al^{3+} and Si^{4+} with ions of lower valence. Mixing SAPs with soil may increase soil aggregation as a result of bridging through cation (Ca^{2+}, Mg^{2+}, Al^{3+}) between the negatively charged groups of SAPs.[14,39] The cations adsorbed on MMT surface may facilitate this cation bridging process, which also contribute to the increasing of soil water stable macro-aggregates.

As shown in Table IV, FP4 shows much better performance in formation of soil water stable macro-aggregates in comparison to BP4. The porous structure of FP products endows them with high surface area, which should increase the probability of SAPs to adsorb cations in soil, consequently facilitating the bridging process between SAPs and soil particles, and leading to soil water stable macro-aggregates enhancement. This presumption was confirmed by SEM images.

Figure 6 shows SEM images of BP4, FP4, and FP9 at different magnifications. As expected, BP4 presented a dense mass structure. Furthermore, FP9 showed more porous structure than FP4, and most of the pores in FP9 were connected to each other to form capillary channels, which explains that soil modified with FP9 has higher water stable macro-aggregates than soil modified with FP4.

It is well known that porous structure enhances the capillary action and enhances the inner-surface area which is beneficial

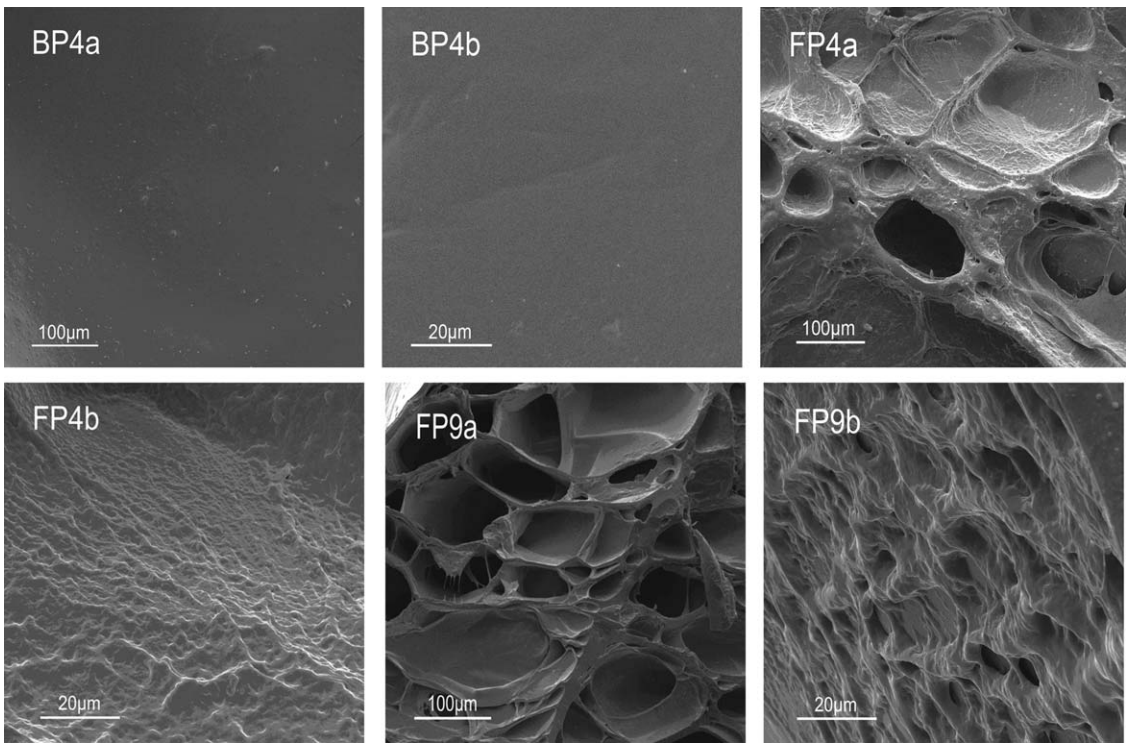

Figure 6. SEM images of BP4, FP4, and FP9 at different magnifications.

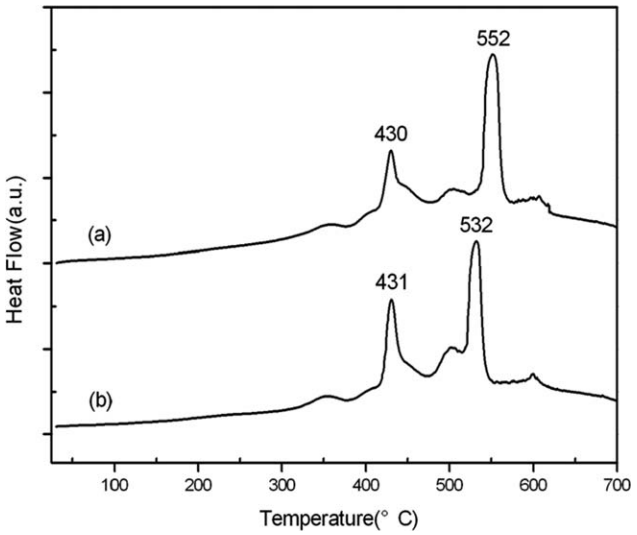

Figure 7. DSC curves of products via FP4 (a) and BP4 (b).

for water absorption, the dramatic enhancements of FP9 in maximum/capillary/field water holding capacity could partly be attributed to its high porous structure.

Thermal Properties Analysis

The DSC thermograms of the FP4 and BP4 samples are exhibited in Figure 7.

Two endothermic peaks were observed in both DSC curves. The peak around 430°C was the endothermic peak by the thermal decomposed carboxyl group removal from the PAA; the other was the peak resulting from the fracture of the PAA main chain. The peak resulting from the fracture of the PAA chain was observed at 552°C for FP4, which was 20°C higher than that of BP4, indicating the better thermal stability of FP samples in comparison with the BP counterparts.

CONCLUSIONS

PAA/MMT/CMC superabsorbent nanocomposites were prepared by FP. CMC played an important role in front propagation and the dispersion degree of MMT. XRD and TEM analysis indicated the nanoscale dispersion of MMT in the composites. FTIR showed that strong chemical bonding existed among MMT, PAA, and CMC molecules. The maximum water absorbency of the optimized product was 643 g/g for distilled water.

Compared with the control soil, soil modified with the nanocomposites showed a significant increase (by 52.4%) in field water holding capacity. The incorporation of small amounts of MMT effectively promoted the formation of soil water stable macro-aggregates. The sample obtained by FP showed much better performance in the formation of soil water stable macro-aggregates, salt resistance, and thermal stability than those obtained by conventional BP. In particular, the dramatic enhancements of soil water stable macro-aggregates for FP samples could be attributed to their porous structures. The above results allow us to conclude that FP can be exploited as a good method for synthesis of SAPs to be used in agriculture.

ACKNOWLEDGMENTS

Authors gratefully acknowledge financial support from the following agencies: Science and Technology Program of Shanxi Province (Grant No. 20110311017-7), Science and Technology Development Program of Jincheng, Shanxi Province (Grant No. 201002065).

REFERENCES

1. Chechilo, N. M.; Khvilivitskii, R. J.; Enikolopyan, N. S. *Dokl. Akad. Nauk.* **1972**, *204*, 1180.
2. Chechilo, N.; Enikolopyan, N. *Dokl. Phys. Chem.* **1974**, *214*, 174.
3. Chechilo, N.; Enikolopyan, N. *Dokl. Phys. Chem.* **1976**, *230*, 840.
4. Pojman, J. A. *Am. Chem. Soc.* **1991**, *113*, 6284.
5. Pojman, J. A.; Ilyashenko, V. M.; Khan, A. M. *J. Chem. Soc. Faraday. Trans.* **1996**, *92*, 2825.
6. Fiori, S.; Malucelli, G.; Mariani, M.; Ricco, L.; Casazza, E. *e-Polymers* **2002**, *57*, 1.
7. Mariani, A.; Alzari, V.; Monticelli, O.; Pojman, J. A.; Caria, G. *J. Polym. Sci. Part A: Polym. Chem.* **2007**, *45*, 4514.
8. Mariani, A.; Fiori, S.; Bidali, S.; Alzari, V.; Malucelli, G. *J. Polym. Sci. Part A: Polym. Chem.* **2008**, *46*, 3344.
9. Mariani, A.; Nuvoli, D.; Alzari, V.; Pini, M. *Macromolecules* **2008**, *41*, 5191.
10. Sannal, R.; Sannal, D.; Alzari, V. *J. Polym. Sci. Part A: Polym. Chem.* **2012**, *50*, 4110.
11. Zhou, J.; Tang, W. Q.; Wang, C. F. *J. Polym. Sci. Part A: Polym. Chem.* **2012**, *50*, 3736.
12. Singha, S.; Singha, M.; Yadav, B. C. *Sensor. Actuat. B: Chem.* **2011**, *160*, 826.
13. Abedi-Koupai, J.; Sohrab, F.; Swarbrick, G. *J. Plant. Nutr.* **2008**, *31*, 317.
14. Bai, W.; Zhang, H.; Liu, B.; Wu, Y.; Song, J. *Soil Use Manage.* **2010**, *26*, 253.
15. Sivapalan, S. *Aust. J. Exp. Agric.* **2006**, *46*, 579.
16. Yan, Q. Z.; Zhang, W. F.; Lu, G. D. *Chem. J. Chin. Univ. Chin.* **2005**, *26*, 1363.
17. Yan, Q. Z.; Zhang, W. F.; Lu, G. D. *Chem.—Eur. J.* **2006**, *12*, 3303.
18. Li, J.; Ji, J.; Xi, J.; Li, B. *Carbohydr. Polym.* **2012**, *87*, 757.
19. Wang, W. B.; Wang, A. Q. *Polym. Adv. Technol.* **2011**, *22*, 1602.
20. Liu, P. S.; Li, L.; Zhou, N. L. *J. Compos. Mater.* **2006**, *23*, 44.
21. Liu, P. H.; Li, L.; Zhou, N. L. *J. Appl. Polym. Sci.* **2006**, *102*, 5725.
22. Qiu, H. X.; Yu, J. G. *J. Appl. Polym. Sci.* **2008**, *107*, 118.
23. Hanks, R. J.; Holmes, W. E.; Tanner, C. B. *Soil. Sci. Soc. Am. J.* **1954**, *18*, 252.

24. Ling, D. Y. Soil Test Guideline; China Forestry Press: Beijing, **2004**; p 66.
25. Yankov, P. *Bulg. J. Agric. Sci.* **2009**, *15*, 393.
26. Kabiri, K.; Hesarian, S.; Zohuriaan-Mehr, M. J. *J. Mater. Sci.* **2011**, *46*, 6718.
27. Pushpamalar, V.; Langford, S. J.; Ahmad, M.; Lim, Y. Y. *Carbohydr. Polym.* **2006**, *64*, 312.
28. Haraguchi, K.; Takehisa, T.; Fan, S. *Macromolecules* **2002**, *35*, 10162.
29. Santiago, F.; Mucientes, A. E.; Osorio, M.; Rivera, C. *Eur. Polym. J.* **2007**, *43*, 1.
30. Meltem, C.; Muserref, O.; Yuksel, S. *J. Appl. Polym. Sci.* **2012**, *123*, 3662.
31. Li, J.; Zhang, X.; Chen, J. *Polym. Chem.* **2009**, *47*, 3391.
32. Liu, J. H.; Wang, W. B.; Wang, A. Q. *Polym. Adv. Technol.* **2011**, *22*, 627.
33. Yu, J.; Shi, J. G.; Dang, P. F.; Mamedov, A. I.; Shainberg, I.; Levy, G. J. *Soil. Sci. Soc. Am. J.* **2012**, *76*, 1758.
34. Bhardwaj, A. K.; Mclaughlin, R. A.; Shainberg, I.; Levy, G. J. *Soil. Sci. Soc. Am. J.* **2009**, *73*, 910.
35. Chatzoudis, G. K.; Rigas, F. *Commun. Soil. Sci. Plan.* **1999**, *30*, 2465.
36. Chen, Z. B.; Dong, F.; Liu, M. Z.; Qi, X. H. *Polym. Eng. Sci.* **2011**, *51*, 2453.
37. Mahdavinia, G. R.; Zohuriaan-Mehr, M. J.; Pourjavadi, A. *Polym. Adv. Technol.* **2004**, *15*, 173.
38. Angers, D. A. *Soil. Tillage. Res.* **1998**, *47*, 9.
39. Paluszek, J. J. *Environ. Stud.* **2010**, *19*, 1287.